frontiers in Materials

ORIGINAL RESEARCH
published: 24 September 2019
doi: 10.3389/fmats.2019.00230

Increasing Exposed Metal Site Accessibility in a Co-MOF-74 Material With Induced Structure-Defects

Jose A. Villajos[1], *Noëmie Jagorel*[1,2], *Stefan Reinsch*[3] *and Franziska Emmerling*[1]*

[1] *Department of Analytical Chemistry, Reference Materials, Federal Institute for Materials Research and Testing (BAM), Berlin, Germany,* [2] *Department of Analytical and Inorganic Chemistry, National Graduate School of Engineering Chemistry of Lille (ENSCL), Lille, France,* [3] *Department of Materials Engineering, Glass, Federal Institute for Materials Research and Testing (BAM), Berlin, Germany*

OPEN ACCESS

Edited by:
Seong Huh,
Hankuk University of Foreign Studies, South Korea

Reviewed by:
Mustafa Ersoz,
Selçuk University, Turkey
Chia-Her Lin,
Chung Yuan Christian University, Taiwan

***Correspondence:**
Franziska Emmerling
Franziska.emmerling@bam.de

Specialty section:
This article was submitted to Colloidal Materials and Interfaces, a section of the journal Frontiers in Materials

Received: *26 February 2019*
Accepted: *05 September 2019*
Published: *24 September 2019*

Citation:
Villajos JA, Jagorel N, Reinsch S and Emmerling F (2019) Increasing Exposed Metal Site Accessibility in a Co-MOF-74 Material With Induced Structure-Defects. Front. Mater. 6:230. doi: 10.3389/fmats.2019.00230

Metal-organic frameworks (MOFs) are promising nanoporous materials with many practical applications. This owes largely to their remarkable porosity and the presence of specific chemical functionalities, such as exposed metal sites (EMS). The MOF-74 structure is known for exhibiting one of the highest EMS densities among porous materials. Moreover, the inclusion of structural defects has been proposed to enhance activity further. This was previously achieved by mixing the original linker together with a second one, having lower topology. The presence of structural defects was evidenced by the resulting crystalline properties and thermal stability. In this work, different mixtures of tetratopic 2,5-dihydroxyterephthalic acid with up to 60% of the tritopic hydroxyterephtalic acid were used to synthesize crystalline Co-MOF-74-like materials. Materials synthesized from higher proportions than 30% of hydroxyterephtalic acid in the synthesis media collapse upon partial removal of the solvent molecules. This indicates the presence of structural defects and the importance of the solvent molecules in stabilizing the crystalline structures. Electron microscope images show that crystal size reduces with inclusion of hydroxyterephtalic acid as the second linker. The presence of coordinated solvent molecules at the EMS was evaluated by Fourier-transform infrared spectra (FTIR) spectroscopy, so that a higher degree of solvent-exchange was observed during washing for defective structures. Furthermore, TG analysis suggests defective structures exhibit lower desolvation temperatures than the defect-free structures. Finally, N_2 adsorption-desorption analyses at −196°C showed an enhanced accessibility of the gas to the inner porosity of the defective structures and therefore, the EMS of the material. All these finding make this pathway interesting to enhance the potential interest of these materials for an industrial application because of both a facilitated activation and a better access to the active sites.

Keywords: MOF-74, structural defects, mixed-linkers, exposed metal sites, facilitated activation

INTRODUCTION

Metal-organic frameworks (MOFs) are porous materials, built by connecting metallic atoms by organic linkers through coordinative bonding (O'Keeffe and Yaghi, 2012). MOFs are highly tunable due to the numerous combinations of metal and organic constituents. Each set of metal and organic constituents exhibits different coordination geometries and topologies, and involves different chemical functionalities (Chughtai et al., 2015). This versatility, together with the development of reticular chemistry, have the potential to design nanomaterials for a better performance toward specific applications (Guillerm et al., 2018). Furthermore, MOFs are known for having extremely large surface areas and void volumes, and generally exhibit low densities (Furukawa et al., 2010). These properties render MOFs particularly suitable for gas storage (Ding and Yazaydin, 2013). In addition, these materials have potential in applications including gas-mixtures separation (Yoon et al., 2010; Lin et al., 2019), catalysis (Li et al., 2015), redox chemistry (Dalapati et al., 2016), or as sensors (Czaja et al., 2009).

For some specific structures, metals are not completely coordinated by linkers. As such, the coordination spheres are typically occupied by solvent molecules during synthesis (Yaghi et al., 2001). These solvent molecules can be subsequently removed by heating or by washing with volatile solvents (Bae et al., 2017). This leads to formation of so-called exposed metal sites (EMS). Recent contributions have demonstrated the usefulness of EMS as active sites for preferential gas adsorption and catalysis (Schlichtenmayer and Hirscher, 2012; Calleja et al., 2014). Amongst porous materials, one of the highest concentrations of EMS can be found in the family M-MOF-74, also known as CPO-27(M), where M is a divalent metal Zn, Mg, Mn, Co, Ni, Cu, Cd, or Fe (Liu et al., 2008; Zhou et al., 2008; Bhattacharjee et al., 2010; Dietzel et al., 2010; Calleja et al., 2014; Diaz-Garcia and Sanchez-Sanchez, 2014). These MOF-74 materials are traditionally made by linking unidimensional rod-like metal-oxide clusters by tetratopic 2,5-dihydroxiterephtalic acid (*dhbdc*) molecules, thus generating a hexagonal network shown in **Figure 1** (Rosi et al., 2005; Xiao and Liu, 2019). Each metal in the cluster is octahedrally coordinated by five oxygen atoms from surrounding linkers, and the sixth position in each octahedron is occupied by a solvent molecule. Removal of this solvent molecule drives formation of EMS (Liu et al., 2008). The EMS in these materials have found application in gas adsorption (Zhou et al., 2008; Dietzel et al., 2010; Xiao and Liu, 2019) and catalysis (Bhattacharjee et al., 2010; Calleja et al., 2014; Xiao and Liu, 2019). The properties of MOF-74 materials have also been tuned by isoreticular modifications, including varying pore size by using larger linkers (Deng et al., 2012), mixing up to ten different metals in the structure (Wang et al., 2014), increasing EMS volumetric density by reducing linker size (Kapelewski et al., 2014), or partitioning the pore size to enhance the confinement of guest molecules (Suh et al., 2017), among others.

Moreover, the surface activity of MOFs has been enhanced by increasing the number of structural defects in their frameworks. Structural defects can improve mass transport, as well as catalytic activity. This owes largely to the aperture of void spaces in the solid frameworks as well as to the increased accessibility of the active sites. Furthermore, structural defects can improve electronic, magnetic and optical properties (Ren et al., 2017). The creation of structural defects has also been studied in MOF-74 structures by mixing the original linker with some terephthalic or benzoic acid derivatives. These derivative linkers exhibit different topologies and are proposed to reduce the coordination degree of metal atoms in the structure (El-Gamel, 2015; Wu et al., 2017). In these works, MOF-74-like structures with induced structural defects were synthesized by using Co, Ni, Mg, or Mn as metals, and their structural properties and CO_2 adsorption behavior were investigated. Therein, it was found that CO_2 adsorption was proportional to the resulting textural properties of the materials, not demonstrating any direct influence of the structural defects in the gas-solid interaction. Here, we investigate the creation of structural defects in a Co-MOF-74 structure by partially mixing the linker *dhbdc* with two modifications of this linker: 2,5-dihydroxybenzoic acid (*dhbz*) and hydroxyterephthalic acid (*hbdc*), as shown in **Figure 1**. The linker *dhbz* was used as a reference since this does not incorporate in the MOF-74 structure (El-Gamel, 2015; Wu et al., 2017). The structural properties of the synthesized materials were compared by powder X-ray diffraction, after different drying-treatments. The presence of EMS-coordinated solvent molecules (N,N-dimethylformamide - DMF- and methanol) was followed by infrared spectroscopy, and the temperature required to remove these solvent molecules was investigated by thermogravimetry. Our results indicate an improvement in the accessibility and activation of the EMS in defective MOF-74 structures, enhancing the potential of this material in applications where EMS are the active sites, such as gas adsorption or catalysis.

MATERIALS AND METHODS

Synthesis of Materials

To synthesize the pure-linker Co-MOF-74 materials (material 0%-b, where b is the second linker), a variation of the published syntheses was implemented (Rowsell and Yaghi, 2006; Botas et al., 2011). In the same, 3.04 mL of a 0.25 M solution of $Co(NO_3)_2{\cdot}6H_2O$ (Aldrich, $\geq$ 98%) was added over 5.0 mL of a 0.052 M solution of 2,5-dihydroxyterepthalic acid (*dhbdc*, Aldrich, 98%), both in DMF (ChemSolute, 99.9%), in a 20 mL glass vial. Then, 1.96 mL of fresh N,N-dimethylformamide (DMF) and 0.5 mL of deionized water were mixed by magnetic stirring for 10 min before sealing the vial. The procedure is similar for the mixed-linker x%-b materials (where x% refers to the molar percentage of the second linker respect to *dhbdc* in the synthesis solution): 0.05·x (in mL) of a 0.052 M solution of *dhbz* (AlfaAesar, 99%) or *hbdc* (Aldrich, 97%) was mixed with 0.05·(100–x) (in mL) of a 0.052 M solution of *dhbdc*, all them in DMF. Syntheses with x from 10 to 100% were carried-out. As an example, to synthesize the material 10%-hbdc, volumes of the DMF-based solutions of *hbdc* (0.50 mL, 0.026 mmol), dhbdc (4.50 mL, 0.23 mmol) and metal (3.04 mL, 0.76 mmol) were mixed, followed by the final addition of 1.96 mL of fresh DMF and 0.5 mL of deionized water to raise the final volume. The molar composition for all synthesis solutions was 0.34 (Linkers):

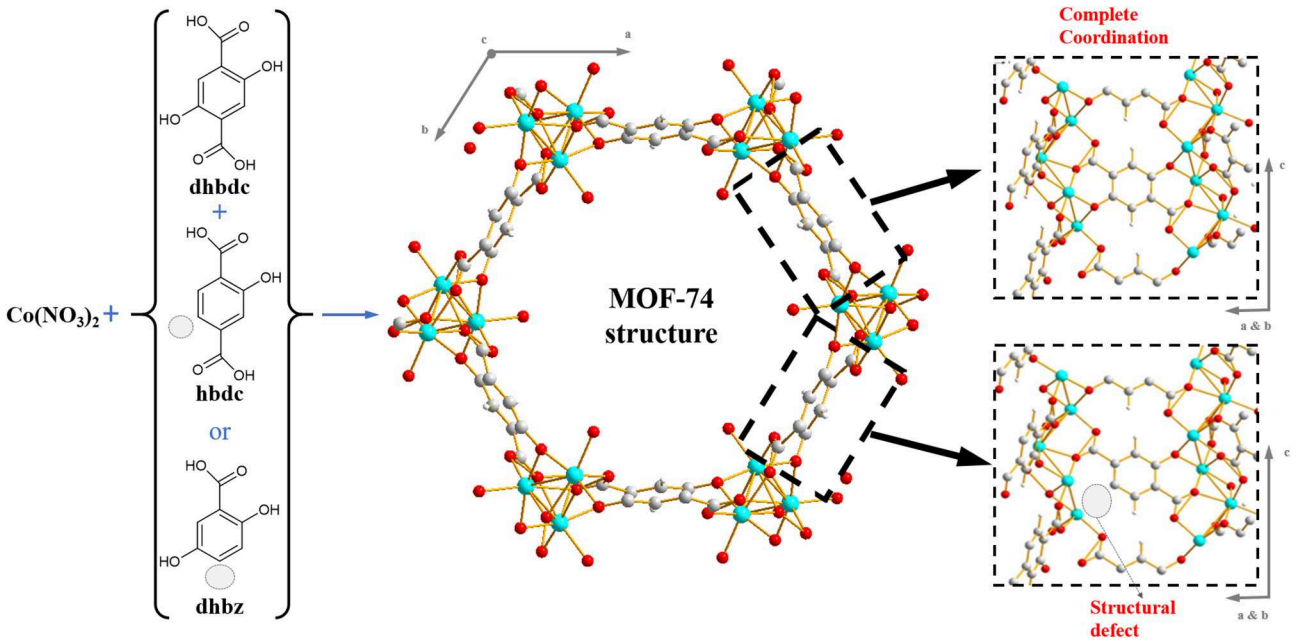

FIGURE 1 | Generation of structural defects in a MOF-74 structure by partial linker substitution.

1 Co: 170 DMF: 1 H_2O. The resulting mixtures were heated at autogenous pressure at 100°C for 20 h to yield dark-brown solids that were recovered by decantation of the hot mother solutions. The obtained crystals were washed with DMF three times and the product was immersed in a large volume of methanol for 6 days. The methanol solution was renewed three times over this period, leading to the formation of dark red materials (x%-b_Me).

The scaled-up syntheses of materials 0%- and 30%-hbdc_SC were performed by a similar procedure, but directly weighing the reagents as solid powders in a glass bottle. 5.52 g (38 mmol) of $Co(NO_3)_2{\cdot}6H_2O$ were mixed with 1.31 g (13 mmol) of *dhbdc* and solved in 250 mL of DMF. Before sealing the autoclave, 12.5 mL of deionized water were also added. The solution was then thermally treated at 100°C for 20 h. For the mixed-linker 30%-hbdc_SC material, the procedure was the same, but 0.90 g of *dhbdc* and 0.35 g of *hbdc* were weighed as organic linker.

Characterization

Powder X-ray diffraction (PXRD) patterns were recorded on a D8 Advanced diffractometer (Bruker AXS, Germany) equipped with a Lynxeye detector, using CuKα ($\lambda = 1.542$ Å) radiation. Samples were measured in reflection geometry in a 2θ range from 5° to 50° with a step size of 0.009°. Scanning electron microscopy (SEM) images were collected using an Environmental Scanning Electron Microscope XL30 ESEM (Thermo Fisher Scientific) at high vacuum. For analysis, samples were covered by 15 nm of Au and SE detector was used. Fourier-transform infrared spectra (FTIR) were recorded for powder samples in transmission mode using an infrared-spectrometer Equinox55, equipped with microscope IR-Scope II (Bruker Optics). The FTIR spectrometer was equipped with an MCT (mercury cadmium telluride) detector and a plate of CaF_2 for a resolution of 2 cm^{-1}. Before analysis, samples were dried in an oven at 80°C overnight and stored in a closed glass vial at room temperature before analysis. Spectra were normalized to the intensity of the signal located at 1,410 cm^{-1} since the corresponding chemical bond to this signal is present in all the used linker molecules. Thermogravimetric analysis (TGA) curves were recorded for the methanol-washed samples in a thermobalance SETARAM TAG 24 (Setaram, Caluire, France) with 1,600°C equipment, in flowing synthetic air (45 mL min^{-1}). For analysis, an initial weight of around 13–19 mg was placed in open corundum crucibles (100 μL) at a heating rate of 2 K min^{-1}. Cooling to room temperature was carried out at −30 K min^{-1} followed by one repetition of this heating and cooling procedure. For correction of buoyancy effect, the second heating cycle was subtracted from the first cycle. N_2 adsorption-desorption isotherms were measured at 77 K on a volumetric ASAP 2020 device (Micromeritics) in the range of relative pressures P/P_0 from 0.0003 to 0.999. For analysis, 0.3 g of each material were loaded in the analysis probe, followed by activation by heating at 150°C for 18 h under a minimum vacuum pressure below 10^{-6} mbar. BET area was calculated by following the Rouquerol method for the selection of the optimal BET P/P_0 range as 0.006–0.02 (Thommes et al., 2015).

RESULTS AND DISCUSSION

The studied materials were synthesized by using different molar proportions (from 10 to 100%) of the organic linkers dihydroxybenzoic acid (*dhbz)* or hydroxyterephthalic acid (*hbdc)* respect to dihydroxyterephthalic acid (*dhbdc)* in the synthesis

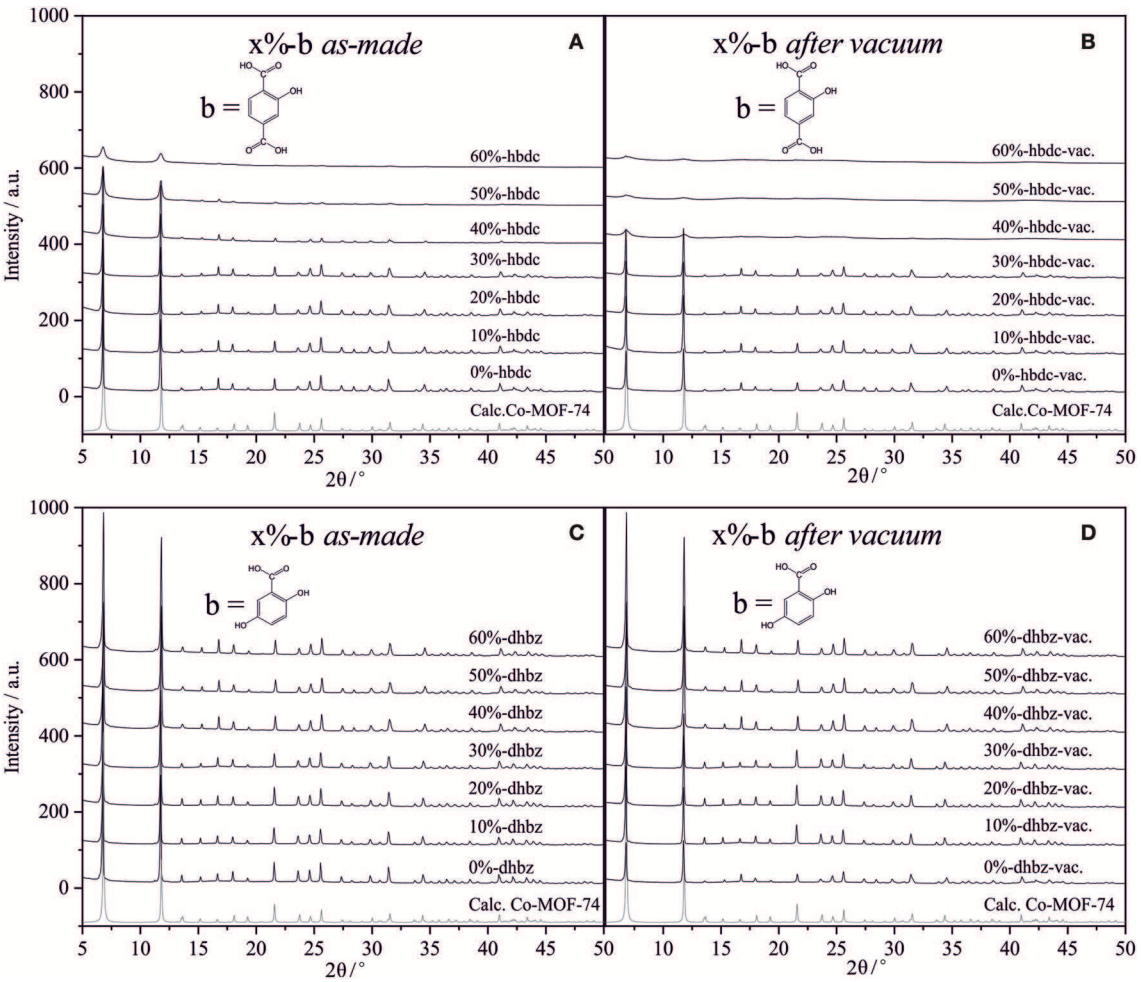

FIGURE 2 | PXRD of the mixed-linker Co-MOF-74 materials using different molar proportions (x) of *hbdc* **(A,B)** or *dhbz* **(C,D)** as the second linker. **(B,D)** correspond to dried in vacuum materials.

media. After the detailed synthesis procedure in the experimental section and before washing with methanol, materials were dried in a fume hood overnight, recovered in a glass vial and weighted. The mass of synthesized solid decreased approximately linearly with increasing amounts of either *dhbz* or *hbdc* as the second linker. However, solid material was successfully recovered in all cases. The only exception was for syntheses involving more than 90% of *dhbz* in the initial solution, for which no solid product was obtained. This could be due to the incorporation of *hbdc* and the lack of *dhbz* in mixed-linker M-MOF-74 materials (M: Mg, Co, Ni, or Mn) that was reported in previous works (El-Gamel, 2015; Wu et al., 2017). A possible explanation for this fact is that hydroxybenzoic acid is a monocarboxylic acid, so this substance could just chelate single metal cations avoiding polymerization. The presence of 10% of the reported amount of *dhbdc* seems to be not enough to yield a solid product.

Figure 2 shows the powder X-ray diffraction (PXRD) patterns of the synthesized materials after substituting up to 60% of the main linker in the synthesis media. The corresponding PXRD patterns are compared to the calculated PXRD pattern of the Co-MOF-74 structure (CSD code: ORIWAP) and to the Co-MOF-74 experimentally synthesized without linker mixture. In the reference phase (i.e., pure Co-MOF-74), the dominant Bragg reflections are found at *ca.* $2\theta = 6.8^\circ$ and 11.7°. Upon inclusion of *hbdc* into the lattice (**Figure 2A**), these reflections remain dominant. However, after using increasing amounts of this second linker, the intensity of all reflections decreases as well as a signal broadening is observed together with a higher amorphous contribution. This suggests a reduction of the crystallinity of the MOF-74 phase in those materials. This qualitative assessment is used to consider the relative crystallinity of the synthesized materials with respect to the reference material. On the other hand, **Figure 2C** confirms the presence of the Co-MOF-74 crystal phase after using any proportion *of dhbz* as the second linker. Almost the same crystallinity was achieved in all materials, without any indication of additional phases being present in the powder sample. This is consistent with the lack of *dhbz*

incorporation in the structure, so pure Co-MOF-74 phase is being synthetized in all cases, similarly to a previous work (Wu et al., 2017).

After drying the materials at ambient-temperature in vacuum overnight, the intensities of the main diffraction signals are further reduced in samples synthesized from ≥40% concentrations of *hbdc* (**Figure 2B**). This indicates that the crystallinity of those materials is notably reduced. The stability of the Co-MOF-74 crystalline structure has been demonstrated in different studies, even after full activation of the EMS in

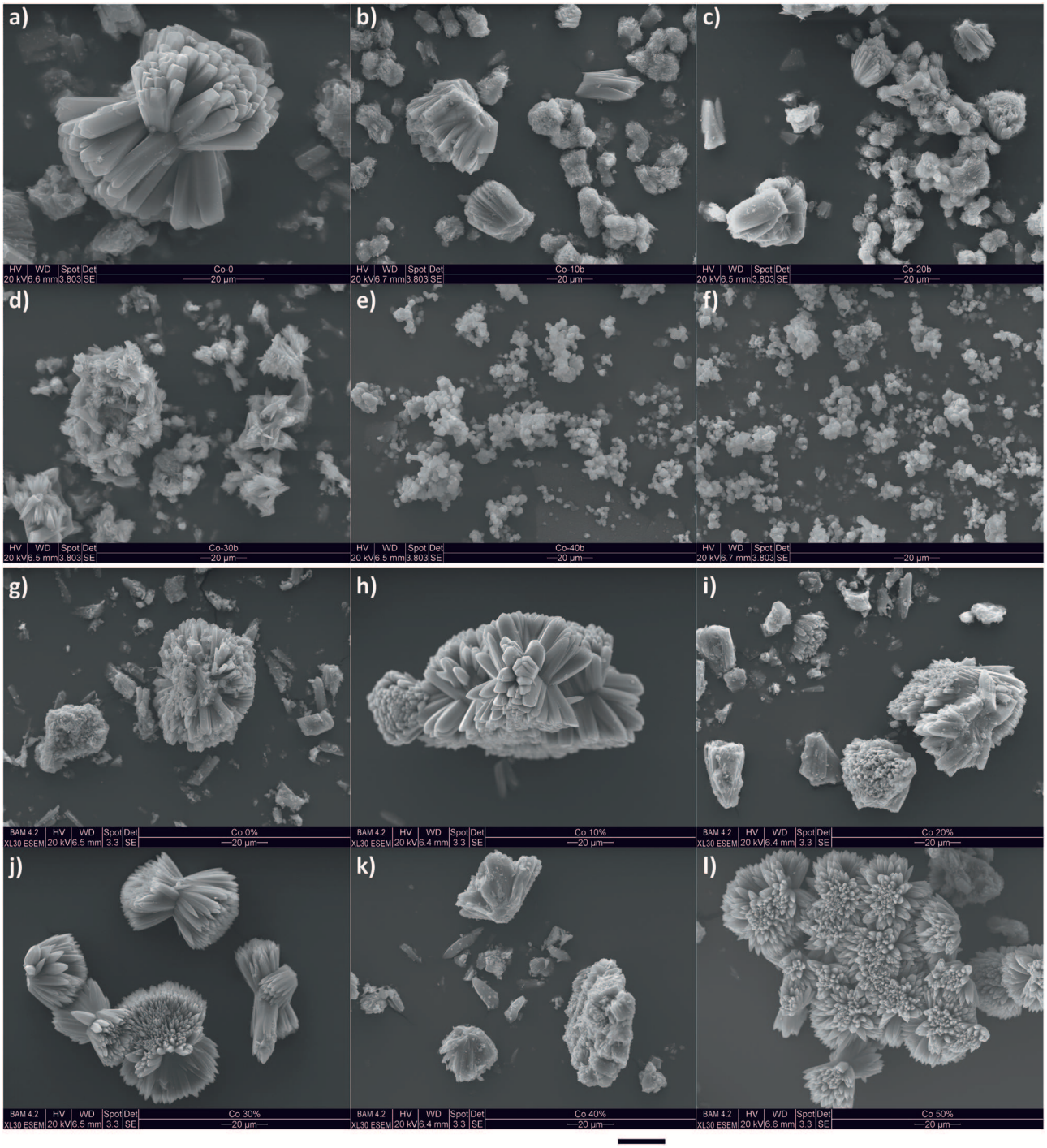

FIGURE 3 | SEM images for some synthesized mixed-linker Co-MOF-74-like materials by using different molar proportions (x) from 0 to 50% of *hbdc* (from **a** to **f**, respectively) or *dhbz* (from **g** to **l**, respectively) as the second linker.

the structure at high temperature (Dietzel et al., 2008, 2010). Therefore, the reduction of crystallinity after drying in vacuum indicates a reduction in the stability of the crystal phase of the material after the partial substitution of its linker. The importance of solvent molecules for maintaining the structural stability of the modified MOF-74 structures can be a direct consequence of the presence of structural defects, that were also assumed in similar works (El-Gamel, 2015; Wu et al., 2017). **Figure 1** depicts how defects are supposed to be created, as a consequence of the mixture of linkers with different topology. The presence of MOF-74 crystal structure implies that metals are in octahedral coordination (Rosi et al., 2005), so that oxygen atoms from the tetratopic linkers occupy five of the six positions in those octahedra. The sixth position is normally occupied by a solvent molecule faced to the cavity, and its removal drives formation of the EMS in a stable network. Since the original linker is mixed with tritopic linker, there must be some metal atoms in the structure where at least two solvent molecules would be necessary. Differently to MOF-74 materials, some MOF structures are not stable after removal of solvents in their coordinatively-unsaturated metal sites (Dietzel et al., 2008). Apparently, the inclusion of these defects after inclusion of higher amounts of the tritopic linker may drive to a higher instability of the framework upon solvent removal. **Figure 2D** shows PXRD patterns that remain unalterable after drying materials where *dhbz* was used as the second linker because there is not incorporation of the benzoic derivative in the structure, since no defects are supposed to be generated in this case.

Figure 3 shows SEM images of mixed-linker materials synthesized by using either *dhbz* or *hbdc* as the second linkers. A general reduction of crystal size is observed when the proportion of *hbdc* as the second linker increases from 0 to 30% (pictures from a to d), although the crystal morphology remains needle-like as expected for Co-MOF-74 (Botas et al., 2011). For larger concentrations of *hbdc* the morphology instead becomes spherical. Samples prepared with *dhbz* as the second linker (pictures from g to l) do not exhibit any significant change in crystal morphology or size, irrespective of *dhbz* concentration. Generally, when using *dhbz*, crystals are larger than those resulting from using *hbdc*. They also exhibit well-defined needle-like morphology in all cases. The latter observation could be related to the lack of incorporation of *dhbz* in the structure. Previous reports have suggested *dhbz* to act as a capping agent or modulator (Sindoro et al., 2014). In that case, the presence of *dhbz* is therefore expected to reduce the free concentration of Co^{2+} in solution. Since these samples are synthesized with a lower concentration of *dhbdc*, this general reduction of reagents presumably slows down the nucleation step, yielding larger crystals. Considering the incorporation of *hbdc* in the structure and the lower synthesis yield for greater proportions of this second linker in the synthesis media, the smaller crystals could indicate that *hbdc* is reducing the rate of crystal growing (Sindoro et al., 2014).

Figure 4 shows the normalized FTIR spectra for the synthesized materials from 0 to 30% of *hbdc* after washing with methanol and drying. Only materials with similar crystallinity

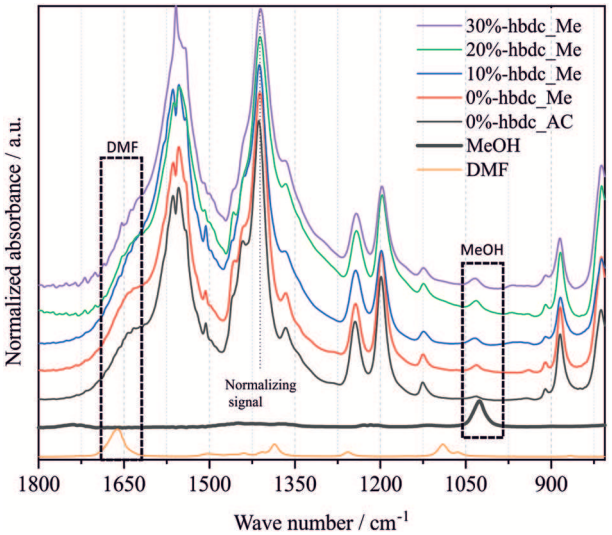

FIGURE 4 | FTIR spectra of the synthesized mixed-linker Co-MOF-74 materials using up to 30% of *hbdc* as the second linker after drying the samples in an oven at 80°C overnight. The sample 0%-hbdc_AC was activated at 150°C and high vacuum for 18 h.

were compared in order to avoid potential changes in spectra due to relative crystallinity. The band located at 1,410 cm^{-1} could correspond to the stretching vibration of the C=C bond of the aromatic ring of the linker, and was previously assigned around 1,485 cm^{-1} for material Mg-MOF-74 (Tan et al., 2014). This chemical bond is always present in the same proportion for all the linkers used in this study. All spectra were therefore normalized to this vibrational band. We noted that normalization with different bands led to the same overall trend, and thus slight intrinsic variation of intensity of the 1,410 cm^{-1} between samples can be neglected. The signal located at 1,662 cm^{-1} corresponds to DMF, and its absorbance signal is lower for higher incorporation of *hbdc* as the second linker. The band at 1,026 cm^{-1} corresponds to methanol, and becomes more pronounced with degree of linker substitution. Considering that the boiling temperature of DMF (153°C) is higher than the temperature used for drying the materials (80°C), the evolution of these two signals indicates a facilitated solvent exchange during the washing with methanol in the defective structures, because of a greater accessibility of DMF in the pores. The presence of methanol in the materials despite heating samples above the boiling temperature of methanol (60°C) indicates the strong interaction of the solvent molecules with the structure, specifically with the EMS as was previously reported (Fu et al., 2012). This interaction makes it necessary to outgas the sample at 150°C and high vacuum for 18 h to remove the methanol molecules (material 0%-hbdc_AC). Previous work demonstrated the absence of this signal in fully-activated MOF-74 materials (Villajos et al., 2015).

Figure 5 compares the thermogravimetric (TG) analysis of Co-MOF-74 and the mixed-linker 30%-*hbdc* material, after washing with methanol. The TG curves show two main weight losses that correspond to solvent removal between 50 and 150°C, and linker combustion above 280°C. The latter leads

to formation of the metal oxide. These temperatures are in accordance with those previously reported for methanol-washed MOF-74 materials (El-Gamel, 2015). The temperature for maximum mass loss rate (minimum of dTG-curves) in the solvent loss is higher than the boiling point of methanol due to strong interactions of solvent with the EMS, as commented above, but also some kinetic effects like diffusion could be involved. By comparing curves from both materials, this temperature is lower for the substituted-linker structure. This indicates that defective MOF-74 materials are more readily activated than the non-defective structures. This is consistent with the FTIR results presented above, where DMF molecules are partially exchanged by methanol molecules. This substitution makes the solvent-removal temperature to decrease. The presence of structural defects and the reduction in the crystal size are other factors that could enhance the mass transport rate.

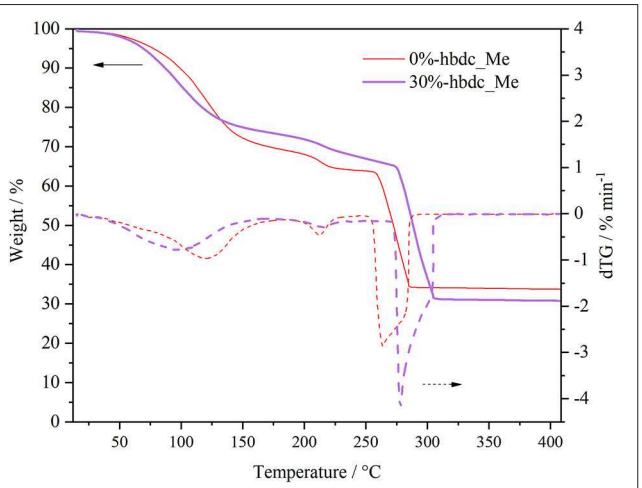

FIGURE 5 | Weight loss and first derivative of weight loss (dTG) of the washed with methanol materials Co-MOF-74 and mixed-linker 30%-hbdc.

Figure 6 shows the N_2 adsorption-desorption isotherms at the temperature of −196°C of the materials 0%- and 30%-hbdc_SC after their activation. Both materials show a type I isotherm corresponding to microporous materials. The isotherm corresponding to material 30%-hbdc_SC shows a higher gas uptake at P/P_0 around 0.2, indicating a higher microporous volume despite a higher crystallinity reduction after analysis (**Figure 6**-inset). A hysteresis loop in the desorption branch and an important high-pressure adsorption ($P/P_0 > 0.95$) are also observed in both materials, reaching a similar value at $P/P_0 = 0.998$. Furthermore, the adsorption and desorption branches do not meet even at lower P/P_0 values than 0.4. These features in the isotherm could indicate lack of equilibrium in the analysis. Similar results were found in mechanochemically synthesized Zn-MOF-74 materials, where a similar effect is a consequence of the presence of non-reacted linker molecules

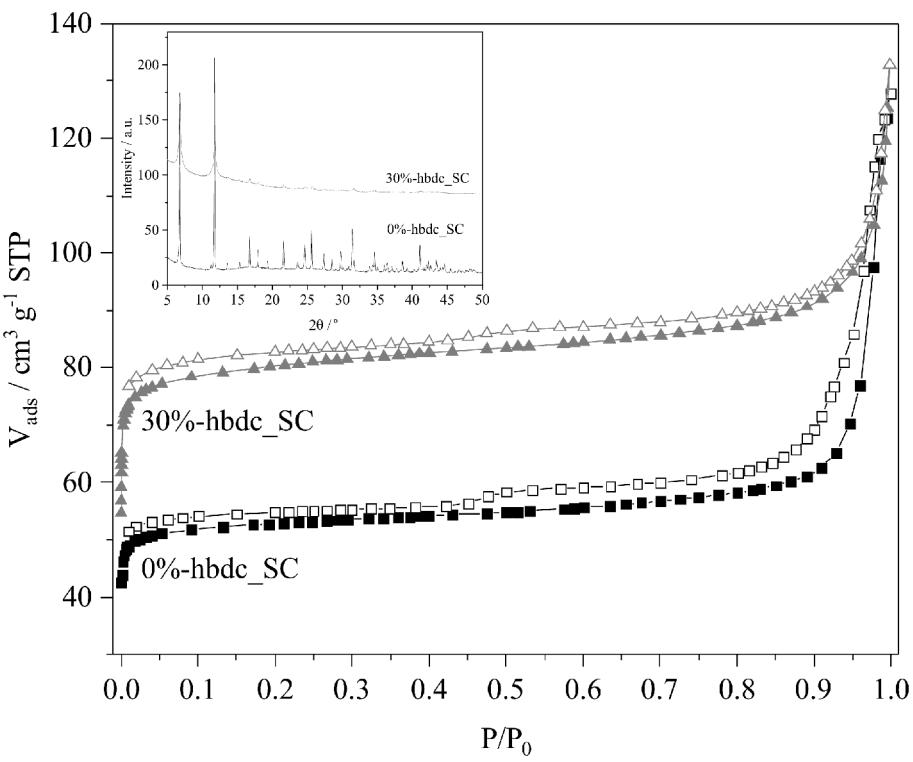

FIGURE 6 | N_2 adsorption-desorption isotherms at −196°C of the scaled-up materials 0%- and 30%-hbdc_SC. Inset: PXRD of the same materials after N_2 adsorption-desorption.

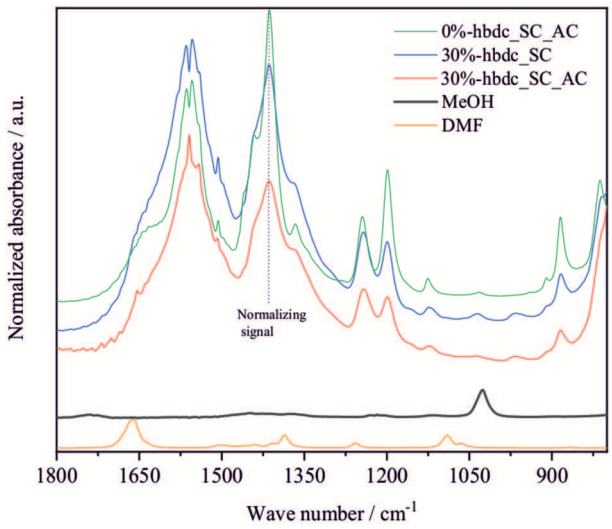

FIGURE 7 | FTIR spectra of the scaled-up materials before and after activation.

blocking the pores (Julien et al., 2016). Herein, materials were solvothermally synthesized and washed several times, so that the presence of unreacted molecules in the pores can be dismissed. The lack of equilibrium might be a consequence of a short time during equilibration and a high initial gas-dose in the analysis. Therefore, in addition to an enhanced accessibility to porous structure due to an improved activation, results are also showing that N_2 diffusion at $-196°C$ is favored in the defective structures. Calculated BET surface areas for the synthesized materials are 215 $m^2\ g^{-1}$ for 0%-hbdc_SC and 323 $m^2\ g^{-1}$ for 30%-hbdc_SC, significantly lower than other values published for Co-MOF-74, usually between 900 and 1,100 $m^2\ g^{-1}$ (Dietzel et al., 2010; Botas et al., 2011; El-Gamel, 2015; Villajos et al., 2015). However, the calculated surface area values in this work are not directly comparable to those higher values because of the above commented lack of equilibrium. **Figure 7** shows that MeOH and, more importantly, DMF signals are reduced up to disappear in the activated 30%-hbdc_SC material. The sample 0%-hbdc_AC still retain a significant amount of DMF after activation in addition to some MeOH molecules. These results confirm a better activation process after the creation of defects, and could be the reason for the improved porous properties that were measured by N_2 adsorption.

CONCLUSION

In summary, Co-MOF-74 materials were synthesized with different proportions of hydroxyterephthalic acid mixed to the original linker (2,5-dihydroxyterephthalic acid) of the structure. This led to the formation of structural defects in the coordination sphere of the metallic sites. A demonstration of the presence of those structural defects is the reduction of crystallinity when materials are dried, which does not occur for pure-linker MOF-74 materials. Despite this, synthesized materials using up to 30% of hydroxyterephthalic acid as the second linker still exhibit the MOF-74 crystal structure. FTIR spectra indicate a better substitution of coordinated DMF to the EMS for methanol after washing the defective structures, and TG analysis suggests a reduction in the temperatures that are required to remove the solvent from pores and activate defective structures. This demonstrates that structural defects involve the coordination of the EMS in the structures and likely enhance their accessibility and facilitate their activation. SEM images show a general reduction in the crystal size for more defective structures, that also facilitates the mass transfer kinetics for the activation. N_2 adsorption-desorption results are according to a better activation of defective structures, but also confirm a better diffusion of the gas molecules to the inner surface of those materials. This is beneficial for applications where EMS are the active sites, since the activation process is a key step that is required prior to usage in e.g., gas-adsorption or catalysis. The severe conditions that are normally used for their laboratory-scale activation are difficult to reproduce at a scaled-up level, so the generation of structural defects can facilitate usage of these materials at an industrial level.

DATA AVAILABILITY STATEMENT

The raw data supporting the conclusions of this manuscript will be made available by the authors, without undue reservation, to any qualified researcher.

AUTHOR CONTRIBUTIONS

NJ performed the synthesis of materials in the laboratory. JV planned the work, prepared the samples for their characterization, and wrote the manuscript. SR performed the TG analysis. FE helped for the discussion of the XRD patterns and contributed to the manuscript writing.

FUNDING

The present work was supported by an internal project from BAM for hydrogen storage in metal-organic framework materials.

ACKNOWLEDGMENTS

We thank to the German Ministry of Economy for financing this research project. Also, to Mrs. A. Kohl (BAM Berlin) for FTIR measurements, to Mrs. I. Feldman (BAM Berlin) for SEM images, to Mr. D. Lubjuhn to Dr. J. Stroh (BAM Berlin) for PXRD measurements, as well as to Dr. M. Maiwald and Dr. A. Michalchuk for general discussions about this work, English assessment, and formal aspects.

REFERENCES

Bae, J., Choi, J. S., Hwang, S., Yun, W. S., Song, D., Lee, J., et al. (2017). Multiple coordination exchanges for room-temperature activation of open-metal sites in metal-organic frameworks. *ACS Appl. Mater. Inter.* 9, 24743–24752. doi: 10.1021/acsami.7b07299

Bhattacharjee, S., Choi, J. S., Yang, S. T., Choi, S. B., Kim, J., and Ahn, W. S. (2010). Solvothermal synthesis of Fe-MOF-74 and its catalytic properties in phenol hydroxylation. *J. Nanosci. Nanotechnol.* 10, 135–141. doi: 10.1166/jnn.2010.1493

Botas, J. A., Calleja, G., Sanchez-Sanchez, M., and Orcajo, M. G. (2011). Effect of Zn/Co ratio in MOF-74 type materials containing exposed metal sites on their hydrogen adsorption behaviour and on their band gap energy. *Int. J. Hydrogen Energy* 36, 10834–10844. doi: 10.1016/j.ijhydene.2011.05.187

Calleja, G., Sanz, R., Orcajo, G., Briones, D., Leo, P., and Martinez, F. (2014). Copper-based MOF-74 material as effective acid catalyst in Friedel Crafts acylation of anisole. *Catal. Today* 227, 130–137. doi: 10.1016/j.cattod.2013.11.062

Chughtai, A. H., Ahmad, N., Younus, H. A., Laypkov, A., and Verpoort, F. (2015). Metal-organic frameworks: versatile heterogeneous catalysts for efficient catalytic organic transformations. *Chem. Soc. Rev.* 44, 6804–6849. doi: 10.1039/C4CS00395K

Czaja, A. U., Trukhan, N., and Muller, U. (2009). Industrial applications of metal-organic frameworks. *Chem. Soc. Rev.* 38, 1284–1293. doi: 10.1039/b804680h

Dalapati, R., Sakthivel, B., Dhakshinamoorthy, A., Buragohain, A., Bhunia, A., Janiak, C., et al. (2016). A highly stable dimethyl-functionalized Ce(IV)-based UiO-66 metal-organic framework material for gas sorption and redox catalysis. *Crystengcomm* 18, 7855–7864. doi: 10.1039/C6CE01704E

Deng, H., Grunder, S., Cordova, K. E., Valente, C., Furukawa, H., Hmadeh, M., et al. (2012). Large-pore apertures in a series of metal-organic frameworks. *Science* 336, 1018–1023. doi: 10.1126/science.1220131

Diaz-Garcia, M., and Sanchez-Sanchez, M. (2014). Synthesis and characterization of a new Cd-based metal-organic framework isostructural with MOF-74/CPO-27 materials. *Micropor. Mesopor. Mater.* 190, 248–254. doi: 10.1016/j.micromeso.2014.02.021

Dietzel, P. D., Georgiev, P. A., Eckert, J., Blom, R., Strassle, T., and Unruh, T. (2010). Interaction of hydrogen with accessible metal sites in the metal-organic frameworks M(2)(dhtp) (CPO-27-M; M = Ni, Co, Mg). *Chem. Commun.* 46, 4962–4964. doi: 10.1039/c0cc00091d

Dietzel, P. D., Johnsen, R. E., Blom, R., and Fjellvag, H. (2008). Structural changes and coordinatively unsaturated metal atoms on dehydration of honeycomb analogous microporous metal-organic frameworks. *Chem. Eur. J.* 14, 2389–2397. doi: 10.1002/chem.200701370

Ding, L. F., and Yazaydin, A. O. (2013). Hydrogen and methane storage in ultrahigh surface area Metal-Organic Frameworks. *Micropor. Mesopor. Mater.* 182, 185–190. doi: 10.1016/j.micromeso.2013.08.048

El-Gamel, N. E. A. (2015). Generation of defect-modulated metal-organic frameworks by fragmented-linker co-assembly of CPO-27(M) frameworks. *Eur. J. Inorg. Chem.* 2015, 1351–1358. doi: 10.1002/ejic.201403110

Fu, Y. Y., Yang, C. X., and Yan, X. P. (2012). Control of the coordination status of the open metal sites in metal-organic frameworks for high performance separation of polar compounds. *Langmuir* 28, 6794–6802. doi: 10.1021/la300298e

Furukawa, H., Ko, N., Go, Y. B., Aratani, N., Choi, S. B., Choi, E., et al. (2010). Ultrahigh porosity in metal-organic frameworks. *Science* 329, 424–428. doi: 10.1126/science.1192160

Guillerm, V., Grancha, T., Imaz, I., Juanhuix, J., and Maspoch, D. (2018). Zigzag ligands for transversal design in reticular chemistry: unveiling new structural opportunities for metal-organic frameworks. *J. Am. Chem. Soc.* 140, 10153–10157. doi: 10.1021/jacs.8b07050

Julien, P. A., Uzarevic, K., Katsenis, A. D., Kimber, S. A., Wang, T., Farha, O. K., et al. (2016). *In situ* monitoring and mechanism of the mechanochemical formation of a microporous MOF-74 framework. *J. Am. Chem. Soc.* 138, 2929–2932. doi: 10.1021/jacs.5b13038

Kapelewski, M. T., Geier, S. J., Hudson, M. R., Stuck, D., Mason, J. A., Nelson, J. N., et al. (2014). M2(m-dobdc) (M = Mg, Mn, Fe, Co, Ni) metal-organic frameworks exhibiting increased charge density and enhanced H2 binding at the open metal sites. *J. Am. Chem. Soc.* 136, 12119–12129. doi: 10.1021/ja506230r

Li, B., Leng, K., Zhang, Y., Dynes, J. J., Wang, J., Hu, Y., et al. (2015). Metal-organic framework based upon the synergy of a Bronsted acid framework and Lewis acid centers as a highly efficient heterogeneous catalyst for fixed-bed reactions. *J. Am. Chem. Soc.* 137, 4243–4248. doi: 10.1021/jacs.5b01352

Lin, R. B., Xiang, S. C., Xing, H. B., Zhou, W., and Chen, B. L. (2019). Exploration of porous metal-organic frameworks for gas separation and purification. *Coordin. Chem. Rev.* 378, 87–103. doi: 10.1016/j.ccr.2017.09.027

Liu, Y., Kabbour, H., Brown, C. M., Neumann, D. A., and Ahn, C. C. (2008). Increasing the density of adsorbed hydrogen with coordinatively unsaturated metal centers in metal-organic frameworks. *Langmuir* 24, 4772–4777. doi: 10.1021/la703864a

O'Keeffe, M., and Yaghi, O. M. (2012). Deconstructing the crystal structures of metal-organic frameworks and related materials into their underlying nets. *Chem. Rev.* 112, 675–702. doi: 10.1021/cr200205j

Ren, J. W., Ledwaba, M., Musyoka, N. M., Langan, H. W., Mathe, M., Liao, S. J., et al. (2017). Structural defects in metal-organic frameworks (MOFs): formation, detection and control towards practices of interests. *Coordin. Chem. Rev.* 349, 169–197. doi: 10.1016/j.ccr.2017.08.017

Rosi, N. L., Kim, J., Eddaoudi, M., Chen, B., O'Keeffe, M., and Yaghi, O. M. (2005). Rod packings and metal-organic frameworks constructed from rod-shaped secondary building units. *J. Am. Chem. Soc.* 127, 1504–1518. doi: 10.1021/ja045123o

Rowsell, J. L., and Yaghi, O. M. (2006). Effects of functionalization, catenation, and variation of the metal oxide and organic linking units on the low-pressure hydrogen adsorption properties of metal-organic frameworks. *J. Am. Chem. Soc.* 128, 1304–1315. doi: 10.1021/ja056639q

Schlichtenmayer, M., and Hirscher, M. (2012). Nanosponges for hydrogen storage. *J. Mater. Chem.* 22, 10134–10143. doi: 10.1039/c2jm15890f

Sindoro, M., Yanai, N., Jee, A. Y., and Granick, S. (2014). Colloidal-sized metal-organic frameworks: synthesis and applications. *Accounts Chem. Res.* 47, 459–469. doi: 10.1021/ar400151n

Suh, B. L., Lee, S., and Kim, J. (2017). Size-Matching Ligand Insertion in MOF-74 for enhanced CO2 capture under humid conditions. *J. Phys. Chem. C* 121, 24444–24451. doi: 10.1021/acs.jpcc.7b08239

Tan, K., Zuluaga, S., Gong, Q. H., Canepa, P., Wang, H., Li, J., et al. (2014). Water reaction mechanism in metal organic frameworks with coordinatively unsaturated metal ions: MOF-74. *Chem. Mater.* 26, 6886–6895. doi: 10.1021/cm5038183

Thommes, M., Kaneko, K., Neimark, A. V., Olivier, J. P., Rodriguez-Reinoso, F., Rouquerol, J., et al. (2015). Physisorption of gases, with special reference to the evaluation of surface area and pore size distribution (IUPAC Technical Report). *Pure Appl. Chem.* 87, 1051–1069. doi: 10.1515/pac-2014-1117

Villajos, J. A., Orcajo, G., Martos, C., Botas, J. A., Villacanas, J., and Calleja, G. (2015). Co/Ni mixed-metal sited MOF-74 material as hydrogen adsorbent. *Int. J. Hydrogen Energy* 40, 5346–5352. doi: 10.1016/j.ijhydene.2015.01.113

Wang, L. J., Deng, H., Furukawa, H., Gandara, F., Cordova, K. E., Peri, D., et al. (2014). Synthesis and characterization of metal-organic framework-74 containing 2, 4, 6, 8, and 10 different metals. *Inorg. Chem.* 53, 5881–5883. doi: 10.1021/ic500434a

Wu, D. F., Yan, W. Q., Xu, H. S., Zhang, E. P., and Li, Q. W. (2017). Defect engineering of Mn-based MOFs with rod-shaped building units by organic linker fragmentation. *Inorg. Chim. Acta* 460, 93–98. doi: 10.1016/j.ica.2016.07.022

Xiao, T., and Liu, D. X. (2019). The most advanced synthesis and a wide range of applications of MOF-74 and its derivatives. *Micropor. Mesopor. Mat.* 283, 88–103. doi: 10.1016/j.micromeso.2019.03.002

Yaghi, O. M., Chen, B. L., and O'Keefe, M. (2001). "Design of open metal sites in porous metal-organic crystals," in *Abstracts of Papers of The American Chemical Society* (Washington, DC: American Chemical Society), U473–U473.

Yoon, J. W., Seo, Y. K., Hwang, Y. K., Chang, J. S., Leclerc, H., Wuttke, S., et al. (2010). Controlled reducibility of a metal-organic framework with coordinatively unsaturated sites for preferential gas sorption. *Angew. Chem. Int. Ed* 49, 5949–5952. doi: 10.1002/anie.201001230

Zhou, W., Wu, H., and Yildirim, T. (2008). Enhanced H2 adsorption in isostructural metal-organic frameworks with open metal sites: strong dependence of the binding strength on metal ions. *J. Am. Chem. Soc.* 130, 15268–15269. doi: 10.1021/ja807023q

Conflict of Interest: The authors declare that the research was conducted in the absence of any commercial or financial relationships that could be construed as a potential conflict of interest.